Supporting Information

Synthesis, structural peculiarities, and photosensitivity of fluorinated dibenzo-1,2,5,6-tetrathiocines†

Alexander A. Buravlev, Alexander Yu. Makarov, Georgy E. Salnikov, Alexander M. Genaev, Irina Yu. Bagryanskaya, Pavel V. Nikulshin, Vyacheslav E. Platonov, and Andrey V. Zibarev

Contents

1. X-ray diffraction

1.1. XRD and DFT molecular geometries

Table S1. Crystallographic data for compounds

Compound	**1**	**2**
Empirical formula	$C_{12}H_4F_4S_4$	$C_{18}F_{16}S_4$
Formula weight	352.39	648.42
Temperature K	296(2)	200(2)
Wavelength Å	0.71073	0.71073
Crystal system	Monoclinic	Monoclinic
Space group	$P2_1/c$	C2/c
Unit cell dimensions *a* Å	4.7996(11)	16.0085(7)
b Å	11.340(3)	11.8439(4)
c Å	12.006(3)	10.6197(4)
α °	90	90
β °	90.465(9)	91.983(2)
γ °	90	90
Volume Å^3	653.4(3)	2012.32(13)
Z	2	4
Density (calcd.) Mg m^{-3}	1.791	2.140
Abs. coefficient mm^{-1}	0.757	0.628
F(000)	352	1264
Crystal size mm^3	0.06 × 0.06 × 0.80	0.20 × 0.20 × 0.40
Θ range for data collection °	3.39-25.12	2.14-26.04
Index ranges	$-5 \le h \le 5$, $-13 \le k \le 13$, $-14 \le l \le 14$	$-19 \le h \le 19$, $-14 \le k \le 14$, $-13 \le l \le 11$
Reflections collected	6275	12137
Independent reflections	1164 R(int) = 0.065	1989 R(int) = 0.051
Completeness to θ %	99.2	99.9
Data / restraints / parameters	1164 / 0 / 91	1989 / 0 / 172
Goodness-of-fit on F^2	1.04	1.05
Final R indices $I > 2\sigma(I)$	$R_1 = 0.0483$, $wR_2 = 0.1361$	$R_1 = 0.0333$, $wR_2 = 0.0820$

Final R indices (all data)	$R_1 = 0.0821$, $wR_2 = 0.1591$	$R_1 = 0.0393$, $wR_2 = 0.0865$
Largest diff. peak/hole e Å^{-3}	0.36 / –0.26	0.51 / –0.34
CCDC	**2347751**	**2347752**

Table S1 (continued). Crystallographic data for compounds

Compound	**17**	**7**
Empirical formula	$C_{12}H_4F_4S_4$	$C_{23}H_{14}F_8S_2$
Formula weight	352.39	506.46
Temperature K	296(2)	200(2)
Wavelength Å	0.71073	0.71073
Crystal system	Monoclinic	Triclinic
Space group	$P2_1/c$	P–1
Unit cell dimensions *a* Å	4.4346(4)	9.0063(5)
b Å	29.235(3)	9.1070(5)
c Å	10.3338(11)	13.7547(7)
α °	90	101.990(2)
β °	100.540(4)	101.874(2)
γ °	90	93.494(2)
Volume Å^3	1317.1(2)	1073.59(10)
Z	4	2
Density (calcd.) Mg m^{-3}	1.777	1.567
Abs. coefficient mm^{-1}	0.751	0.326
F(000)	704	512
Crystal size mm^3	0.10 × 0.20 × 0.80	0.40 × 0.50 × 0.80
Θ range for data collection °	2.9-27.6	3.05 – 26.20
Index ranges	$-5 \le h \le 4$, $-37 \le k \le 38$, $-13 \le l \le 13$	$-19 \le h \le 19$, $-14 \le k \le 14$, $-13 \le l \le 11$
Reflections collected	13123	11516
Independent reflections	3042 R(int) = 0.052	4246 R(int) = 0.051
Completeness to θ %	99.8	99.6
Data / restraints / parameters	3042 / 0 / 181	4246 / 0 / 298
Goodness-of-fit on F^2	1.02	1.02
Final R indices $I > 2\sigma(I)$	$R_1 = 0.0410$, $wR_2 = 0.0905$	$R_1 = 0.0476$, $wR_2 = 0.1257$
Final R indices (all data)	$R_1 = 0.0580$, $wR_2 = 0.0985$	$R_1 = 0.0618$, $wR_2 = 0.1372$

Largest diff. peak/hole e Å^{-3}	0.30 / –0.21	0.36 / –0.24
CCDC	**2351030**	**2351029**

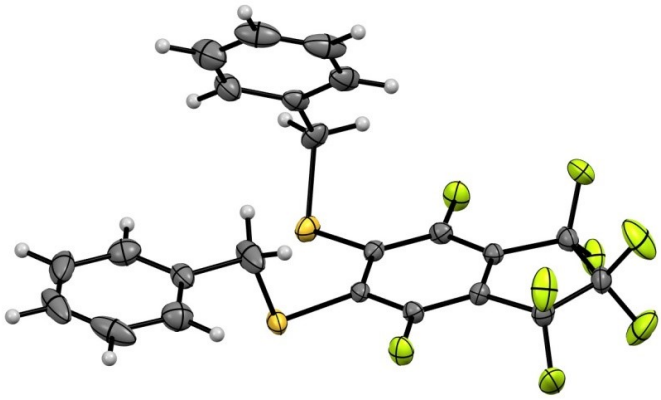

Figure S1 XRD molecular structure of **7** (CCDC 2351029) shown in thermal displacement ellipsoids of 30% probability. Colour code: C – grey, H – light grey, F – green, S – orange.

Table S2. Fully-optimized B3LYP/DKH-def2-qzvpp and XRD molecular geometry of compound **1**

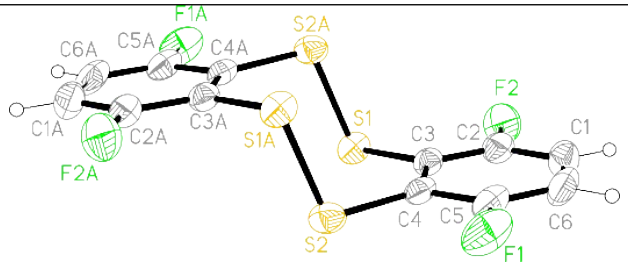

Bond length, Å			Angle value, º		
Bond	DFT	XRD	Bond angle	DFT	XRD
C1–C2	1.383	1.3623	C8–C7–S3	123.49	123.30
C1–C3	1.385	1.357	C7-S3–S1	103.22	103.29
C1–H1	1.080	–	S3–S1–C5	103.21	102.83
C10–C12	1.385	1.357	S1–C5–C6	123.49	122.47
C10–F4	1.342	1.352	C5–C6–S2	123.49	123.30
C11–C12	1.383	1.363	C6–S2–S4	103.22	103.29
C11–H3	1.080	–	S2–S4–C8	103.21	102.83
C12–H4	1.080	–	S4–C8–C7	123.49	122.47
C2–C4	1.385	1.365	Torsion angle	Angle value, º	
C2–H2	1.080	–	C8–C7–S3–S1	81.09	82.85

C3–C5	1.393	1.386	C7–S3–S1–C5	–110.94	–112.24
C3–F1	1.342	1.352	S3–S1–C5–C6	81.02	79.91
C4–C6	1.393	1.393	S1–C5–C6–S2	0.03	1.21
C4–F2	1.342	1.345	C5–C6–S2-S4	–81.09	–82.85
C5–C6	1.411	1.408	C6–S2–S4–C8	110.94	112.24
C5–S1	1.773	1.768	S2–S4–C8–C7	–81.02	–79.91
C6–S2	1.773	1.760	S4–C8–C7–S3	–0.03	–1.21
C7–C8	1.411	1.408			
C7–C9	1.393	1.393			
C7–S3	1.773	1.760			
C8–C10	1.393	1.386			
C8–S4	1.773	1.768			
C9–C11	1.385	1.365			
C9–F3	1.342	1.345			
S1–S3	2.079	2.057			
S2–S4	2.079	2.057			

Table S3. Fully-optimized B3LYP/DKH-def2-qzvpp and XRD molecular geometry of compound **2**

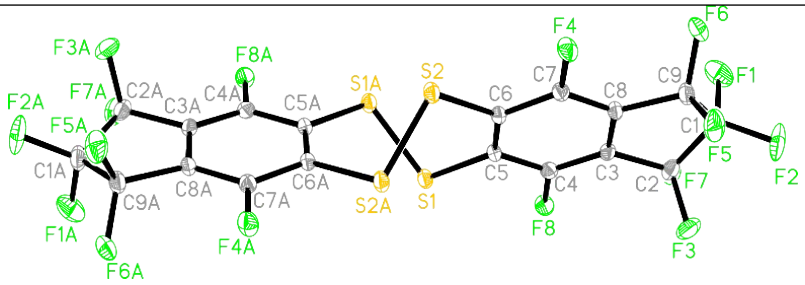

Bond length, Å			Angle value, º		
Bond	DFT	XRD	Bond angle, º	DFT	XRD
C1–C2	1.568	1.534	C11–C10–S3	126.21	126.27
C1–C3	1.568	1.544	C10–S3–S2	103.46	101.95
C1–F1	1.340	1.327	S3–S2–C9	103.58	101.95
C1–F2	1.349	1.354	S2–C9–C8	126.27	126.27
C10–C11	1.412	1.397	C9–C8–S1	126.21	125.94
C10–C12	1.398	1.768	C8–S1–S4	103.39	103.14
C10–S3	1.769	1.416	S1–S4–C11	103.53	103.14
C11–C13	1.398	1.393	S4–C11–C10	126.29	125.94

C11–S4	1.769	1.771	C11–C10–S3	126.21	126.27
C12–C14	1.377	1.369	Torsion angle	Angle value, º	
C12–F9	1.337	1.343	C11–C10–S3–S2	–45.02	–44.01
C13–C15	1.377	1.369	C10–C11–S4–S1	–44.75	–42.57
C13–F10	1.337	1.347	C8–C9–S2–S3	–44.86	–44.01
C14–C15	1.391	1.388	C9–C8–S1–S4	–45.28	–42.57
C14–C16	1.499	1.499	C10–S3–S2–C9	114.71	115.78
C15–C17	1.500	1.506	C8–S1–S4–C11	114.82	113.44
C16–C18	1.568	1.544	C11–C10–C9–C8	60.18	63.69
C16–F11	1.351	1.359			
C16–F12	1.362	1.335			
C17–C18	1.568	1.534			
C17–F13	1.351	1.362			
C17–F14	1.362	1.339			
C18–F15	1.349	1.354			
C18–F16	1.340	1.327			
C2–C4	1.499	1.506			
C2–F3	1.362	1.339			
C2-F4	1.351	1.362			
C3–C5	1.499	1.499			
C3–F5	1.362	1.335			
C3–F6	1.351	1.359			
C4–C5	1.392	1.388			
C4–C6	1.377	1.369			
C5–C7	1.377	1.369			
C6–C8	1.398	1.393			
C6–F7	1.337	1.347			
C7–C9	1.398	1.397			
C7–F8	1.337	1.343			
C8–S1	1.769	1.771			
C8–C9	1.412	1.416			
C9–S2	1.769	1.768			
S1–S4	2.056	2.044			
S2–S3	2.057	2.036			

1.2. Crystal packing

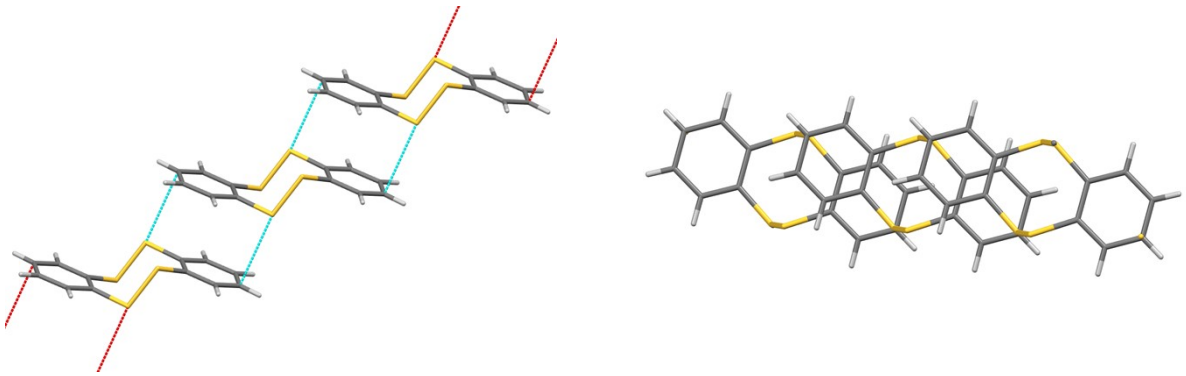

4, C…S shortened contacts in the presence of π-stacking interactions

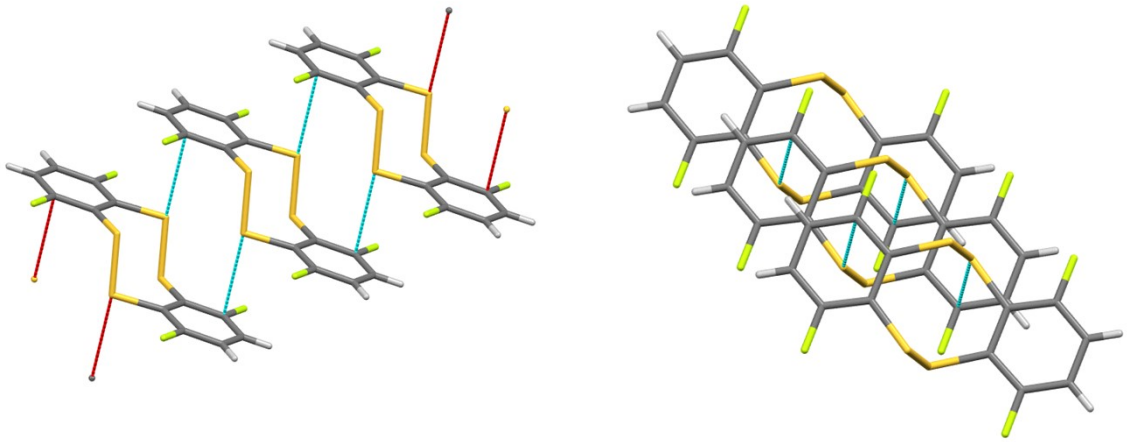

1, C…S shortened contacts in the absence of π-stacking interactions

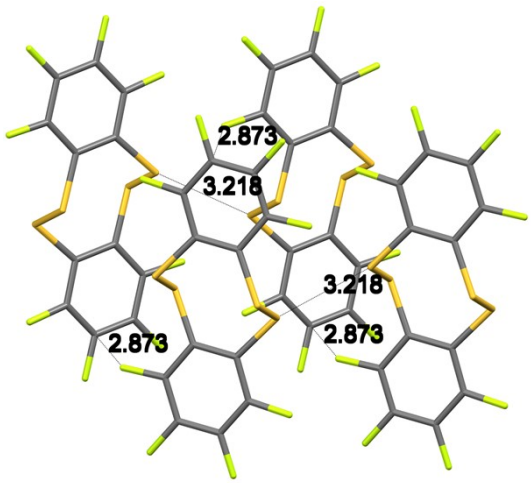

α-**5**, shortened intermolecular contacts

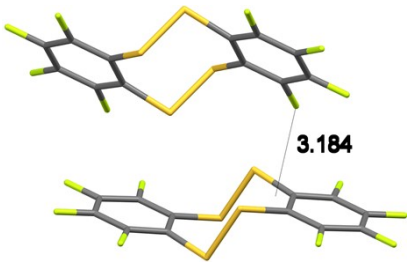

α-**5**, F…π interactions

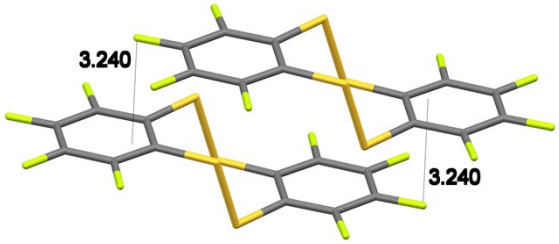

β-**5**, F…π interactions

Figure S2 Fragments of crystal packing of **1**, **4**,[S1] and **5**.[S2]

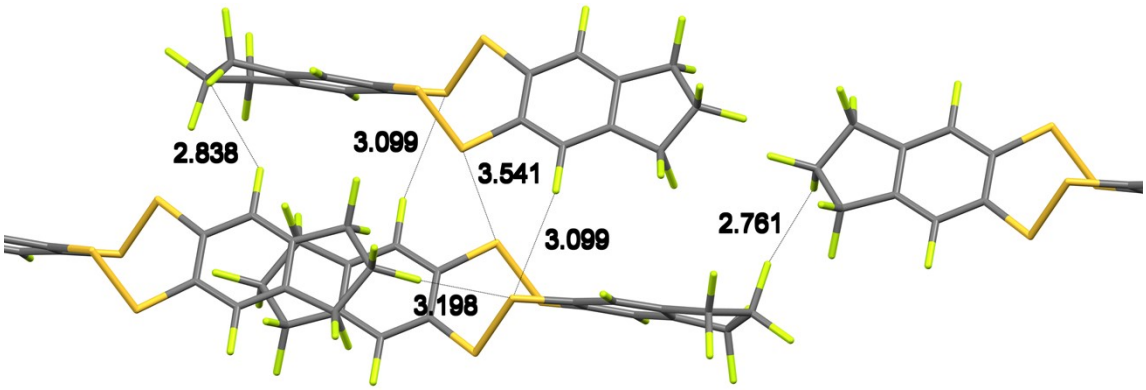

Figure S3 Fragments of crystal packing of **2** featuring shortened intermolecular contacts / SBIs.

2. Spectral calculations

2.1. NMR spectra

According to the DFT calculations with CPCM solvent corrections, both δ^{1}H and δ^{19}F of the *chair* conformer of **1** are downfield relative to those of the *twist* conformer (Table S4). At the BP86/def2-tzvpp level of theory, the *twist* conformer is more stable than the *chair* conformer by ~4.67 kJ mol^{-1}. At 296 K in $CDCl_3$ solution, in ^{19}F NMR spectra the ratio of the conformers is 1:1.3, and in ^{1}H NMR spectra 1:1.2, in favor of the twist one; for the ^{1}H NMR data, accuracy is reduced because of overlapping of the signal of residual H atoms of $CDCl_3$ with the signal of the chair conformer.

Table S4. Experimental and DFT-calculated chemical shifts (δ, ppm) of compound **1** for solutions in $CDCl_3$

				$\delta^{19}F^{a}$				
					B3LYP			wB97X-V
Conformer	exp.	def2-tzvpp	def2-tzvppd	def2-qzvpp	DKH-def2-qzvpp	pcSseg-3	IGLO-III	IGLO-III
chair	–104.2	–98.8	–100.6	–99.6	–99.5	–99.4	–100.4	–105.5
twist	–110.4	–105.7	–107.9	–106.9	–106.8	–107.8	–108	–112.9
					PBE0			
					DKH-def2-qzvpp		IGLO-III	
chair	–104.2					–98.3		–101.8
twist	–110.4					–105.7		–109.6
				$\delta^{1}H^{b}$				
					B3LYP			wB97X-V
Conformer	exp.	def2-tzvpp		def2-qzvpp	DKH-def2-qzvpp	pcSseg-3	IGLO-III	IGLO-III
chair	7.21	7.65		7.65	7.65	7.68	7.63	7.99
twist	7.00	7.44		7.42	7.43	7.43	7.42	7.79
					PBE0			
					DKH-def2-qzvpp		IGLO-III	
chair	7.21				7.71		7.67	
twist	7.00				7.47		7.45	
				$\delta^{13}C^{b}$				
					PBE0			
		exp.		def2-tzvpp	IGLO-III	pcSseg-3		
	C–H	119.3		120.5	120.1	120.1		
chair	C–F	158.8		162.2	161.9	162.0		
	C–S	– [c]		132.2	132.4	131.9		
	C–H	114.1		114.5	114.0	113.9		
twist	C–F	157.2		160.3	160.0	160.2		
	C–S	– [c]		124.6	124.7	124.2		

[a] Relative to $CFCl_3$. [b] Relative to TMS. [c] Not detected due to low intensity.

According to the DFT calculations for compound **2** with CPCM solvent corrections (Table S5), the signal with $\delta^{19}F$ = –103.9, as well as the two AB systems formed by pairs of signals with $\delta^{19}F$ = –107.3 and –108.2 (J_{AB}^{exp} = 268, $J_{AB}^{PBE0/pcJ-3}$ = 247 Hz), and –128.6 and –129.5 (J_{AB}^{exp} = 242, $J_{AB}^{PBE0/pcJ-3}$ = 210 Hz), belong to the *chair* conformation. The signal with $\delta^{19}F$ = –109.1, the AB system formed by the signals with $\delta^{19}F$= –106.8 and –107.4 (J_{AB}^{exp} = 268, $J_{AB}^{PBE0/pcJ-3}$ = 240 Hz), and the singlet with $\delta^{19}F$ = –129.1 belong to the *twist* conformation. The calculations confirm that in toluene AB systems for both conformations are possible at the α-CF_2 groups, and only for the *chair* conformation at the β-CF_2 groups. At the PBE0/def2-tzvpp level of theory, the *twist* conformer is more stable than the *chair* conformer by ~8.68 kJ mol^{-1}. At 296 K, experimental ratio of the conformers is 1:7.1 in favor of the twist one.

Table S5. Experimental and DFT-calculated chemical shifts of compound **2** in toluene ($-\delta^{19}F$, ppm; relative to $CFCl_3$)

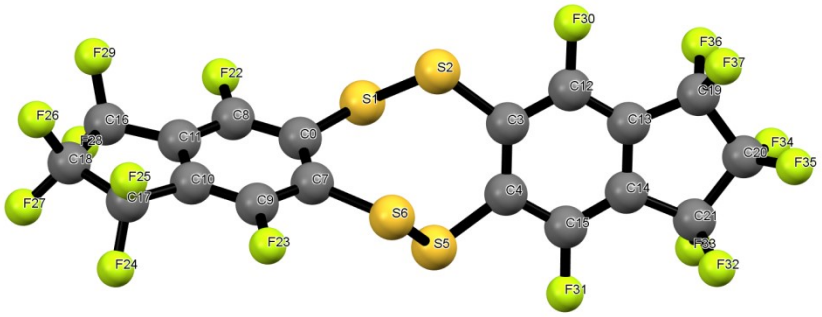

$-\delta^{19}F$

Atom	experiment		B3LYP					
			def2-tzvpp		IGLO-III		pcSseg-2	
	chair	*twist*	*chair*	*twist*	*chair*	*twist*	*chair*	*twist*
F22	103.9	109.1	110.9	117.4	113.0	120.5	112.4	119.1
F23	103.9	109.1	110.8	117.4	113.0	120.4	112.5	119.1
F30	103.9	109.1	110.8	117.4	113.0	120.4	112.4	119.1
F31	103.9	109.1	110.9	117.4	113.0	120.5	112.4	119.1
F24	107.3	106.8	115.8	113.9	116.4	115.1	118.1	116.3
F28	107.3	106.8	115.7	113.9	116.3	115.1	118.0	116.3
F32	107.3	106.8	116.1	113.9	116.8	115.1	118.5	116.3
F37	107.3	106.7	116.2	113.9	117.1	115.1	118.7	116.3
F25	108.2	107.4	116.3	116.2	117.1	117.4	118.7	118.8
F29	108.2	107.4	116.0	116.2	116.9	117.4	118.6	118.8
F33	108.2	107.4	116.5	116.2	117.4	117.4	119.0	118.8
F36	108.2	107.5	116.5	116.2	117.4	117.4	119.1	118.8
F26	128.6	129.1	136.9	136.4	136.6	136.8	138.5	138.2
F34	128.6	–129.1	136.7	136.4	136.6	136.8	138.5	138.2
F27	129.5	–129.1	136.8	136.4	136.8	136.8	138.7	138.2
F35	129.5	–129.1	136.9	136.4	136.8	136.8	138.7	138.2

	experiment		PBE0					
			def2-tzvpp		IGLO-III		pcSseg-2	
	chair	*twist*	*chair*	*twist*	*chair*	*twist*	*chair*	*twist*
F22	103.9	109.1	101.9	108.9	104.3	112.1	102.6	109.7
F23	103.9	109.1	102.2	108.9	104.8	112.0	103.1	109.7
F30	103.9	109.1	101.7	108.9	104.3	112.1	102.6	109.7
F31	103.9	109.1	102.3	108.9	104.8	112.1	103.0	109.7
F24	107.3	106.8	111.3	109.6	112.7	111.2	113.2	111.6

F28	107.3	106.8	111.2	109.6	112.7	111.2	113.2	111.6
F32	107.3	106.8	111.8	109.6	113.4	111.2	113.9	111.6
F37	107.3	106.8	111.6	109.6	113.4	111.2	113.8	111.6
F25	108.2	107.4	111.8	112.2	113.6	113.8	114.0	114.4
F29	108.2	107.4	111.8	112.2	113.6	113.8	114.0	114.4
F33	108.2	107.4	112.3	112.2	114.2	113.8	114.6	114.4
F36	108.1	107.5	112.2	112.2	114.0	113.8	114.5	114.4
F26	128.6	129.1	132.2	131.9	133.0	132.8	133.6	133.4
F34	128.6	129.1	132.0	131.9	132.8	132.8	133.5	133.4
F27	129.5	129.1	132.3	131.9	133.1	132.8	133.8	133.4
F35	129.5	129.1	132.2	131.9	133.1	132.8	133.8	133.4
	experiment		wB97M-V					
			def2-tzvpp		IGLO-III		pcSseg-2	
	chair	*twist*	*chair*	*twist*	*chair*	*twist*	*chair*	*twist*
F22	103.9	109.1	88.5	95.1	96.4	103.3	94.7	100.9
F23	103.9	109.1	87.8	95.1	95.8	103.3	94.1	100.9
F30	103.9	109.1	88.5	95.1	96.5	103.3	94.7	100.9
F31	103.9	109.1	87.9	95.1	95.8	103.3	94.1	100.9
F24	107.3	106.8	90.1	87.8	94.0	91.9	94.3	92.2
F28	107.3	106.8	90.1	87.8	93.9	92.8	94.2	92.2
F32	107.3	106.8	89.6	87.8	93.8	91.9	94.2	92.2
F37	107.3	106.7	89.9	87.8	94.2	91.9	94.4	92.2
F25	108.2	107.4	89.9	89.4	94.2	93.5	94.4	93.8
F29	108.2	107.4	89.4	89.4	93.8	93.5	94.2	93.9
F33	108.2	107.4	89.5	89.4	93.9	93.5	94.3	94.0
F36	108.2	107.5	89.5	89.4	93.9	93.5	94.3	94.0
F26	128.6	129.1	109.6	108.9	113.0	112.5	113.6	112.9
F34	128.6	129.1	109.6	108.9	112.9	112.5	113.5	112.9
F27	129.5	129.1	109.3	108.9	113.0	112.5	113.5	112.9
F35	–33.4	–33.8	–53.5	–54.0	–49.8	–50.4	–49.3	–50.0

According to the DFT calculations with CPCM corrections on compound **5** (Table S6), the signals with $\delta^{19}F$ = –123.1 and –148.5 ppm correspond to the *chair* conformation; while those with $\delta^{19}F$ = –131.3 and –155.5, to the *twist* conformation. At the PBE0/def2-tzvpp level of theory with CPCM corrections for $CHCl_3$ solvent, the *chair* conformer is more stable than the *twist* conformer by 4.83 kJ mol^{-1}; and the experimental ratio of the conformers at 296 K approximately is ~1:5 in favor of the *chair* conformer.

Table S6. Experimental and DFT-calculated chemical shifts of compound **5** in chloroform (–δ^{19}F, ppm; relative to $CFCl_3$)

Atom	–δ^{19}F							
	Experiment		PBE0					
			def2-tzvpp		IGLO-III		pcSseg-2	
	chair	*twist*	*chair*	*twist*	*chair*	*twist*	*chair*	*twist*
$F^{1,4,7,10}$	123.1	131.3	119.3	128.7	119.9	130.1	118.6	127.9
$F^{2,3,8,9}$	148.5	155.5	146.5	155.5	146.6	155.7	146.4	155.5

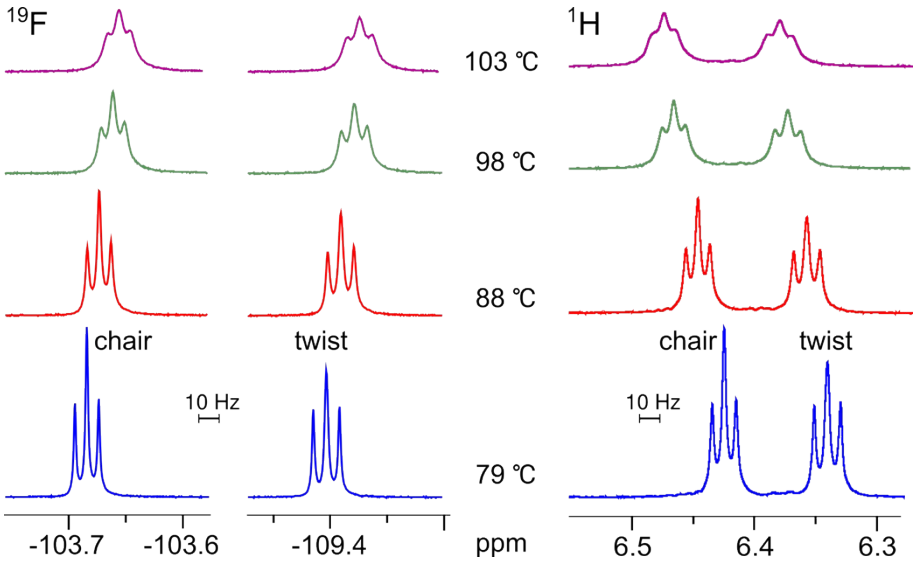

Figure S4 Variable-temperature ^{1}H and ^{19}F NMR spectra of **1** in toluene solution.

The $^{19}F\{^1H\}$ NMR spectrum of **17** consists of two symmetric doublet doublets at δ –99.7 ppm and –104.9 ppm (Figure S5) and resembles a typical first order spectrum of an AA'XX' spin system having coupling constants $J_{AX} = J_{A'X'} = 8.7$ Hz and $J_{AX'} = J_{A'X} = 7.1$ Hz. Taking into account the spin system symmetry, one should assign $^5J_{AX}$ to the coupling between the ^{19}F nuclei in the *para* positions to each other, while $^7J_{AX'}$ to the coupling between the two ^{19}F nuclei belonging to different aromatic rings. However, such a set of coupling constants, particularly the excessively large value of the long range $^7J_{AX'}$, would be hardly possible for fluoroarenes.[S3,S4] Therefore, the spectrum was analyzed as a second-order one using common analytical treatment for the AA'XX' spin system.[S5] After expanding the expressions for transition frequencies in Taylor series up to 2nd order and discarding small $J_{AA'}$, $J_{AX'}$ and $J_{A'X}$ followed by simplifications, the approximation was obtained for the J_{AX} coupling constant as the distance

between the two outer components of the multiplet, $J_{AX} = J_{A'X'}$ ~15.7 Hz. Then from the distance between the two inner multiplet components, 1.6 Hz, which should be ~$J_{AX}^2/2J_{XX'}$, the larger coupling constant $J_{XX'}$ ~77 Hz was estimated. Then, according to spin system treatment, a search was performed for the two much less intense transitions located at the distance of J_{XX} ~77 Hz to the left and right from the multiplet centre, with expected intensity ~$(J_{AX}/2J_{XX'})^2$ ~1% of the main multiplet components. Indeed, there are two very small peaks of approximately that intensity. With strict iterative numerical fitting procedure,[S6] the final spin system parameters were derived: coupling constant between the ^{19}F nuclei in the *para* positions to each other J_{AX} = $J_{A'X'}$ = 15.7 Hz, and the large «through-space» coupling constant[S7,S8] $J_{XX'}$ = 73.7 Hz. These assignments are supported by XRD data and quantum chemical modeling, according to which the F_X and $F_{X'}$ atoms are spatially close to each other (Figure S5).

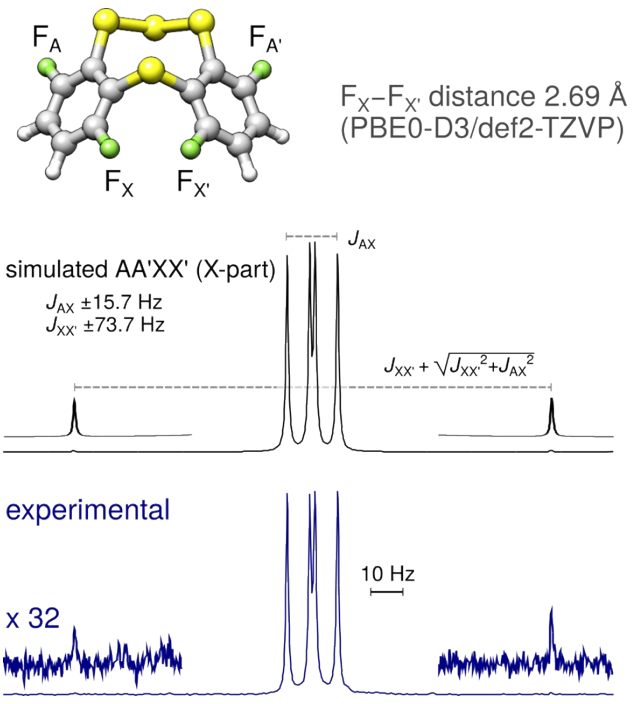

Figure S5 Molecular geometry of **17**, together with its experimental and simulated ^{19}F{^{1}H} NMR spectra (downfield multiplet, δ –99.7 ppm). The F_X…$F_{X'}$ distance is ~0.2 Å shorter than the sum of VdW radii. Colour code: C – grey, H – light grey, F – green, S – yellow.

2.2. UV-Vis spectra

According to the TD-DFT calculations, the *chair* conformation of **1** has more intensive absorption in the long-wave region; whereas the *twist* conformation, in the short-wave region. For **2** and **5**, the situation is similar though less pronounced (Figure S6).

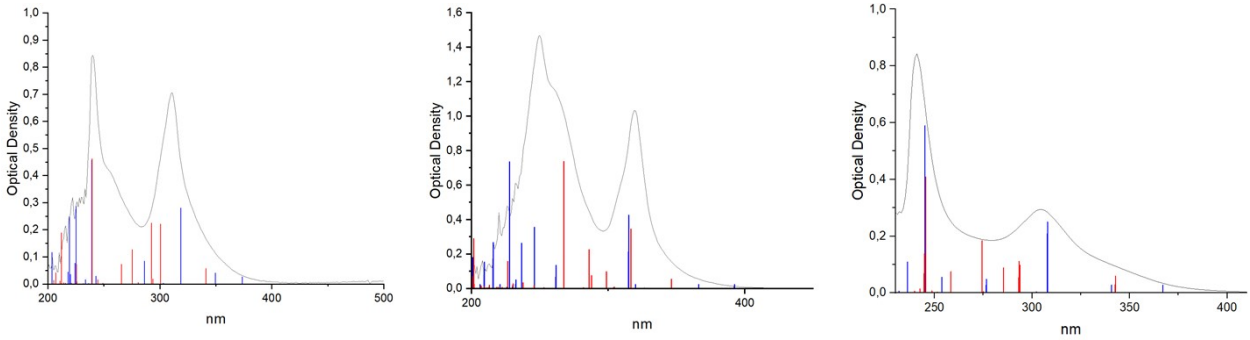

1 **2** **5**

Figure S6 Experimental UV-Vis spectra of **1**, **2** and **5** in chloroform solution (black lines) and positions and relative intensities of TD-B3LYP/def2-tzvpp calculated electronic transitions of the *chair* (blue bars) and *twist* (red bars) conformers.

2.3. IR spectra

The IR spectra of **1** and **2** were calculated at the B3LYP/DKH-def2-qzvpp level of theory; and the spectrum of **17**, at the PBE0/DKH-def2-qzvpp level of theory. The scaling factors were 0.948, 0.985, and 0.955, respectively (Figure S7).

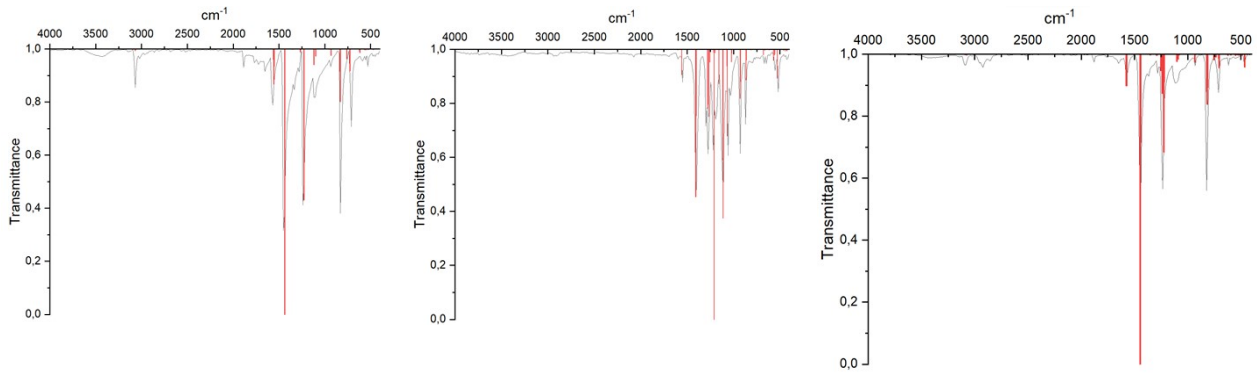

1 **2** **17**

Figure S7 Experimental in KBr pellets (black lines) and DFT-calculated (red bars) IR spectra of **1**, **2**, and **17**.

3. Quantum chemical calculations for conformational analysis

3.1. Selection of computational method

To study the PES, including Hessian calculations, the TS searches, and their connection to the minima via IRC, the well-established PBE/L1 method, the modern fast and accurate r^{2}SCAN-3c method,[S9] and the standard DFT method PBE0-D3/def2-tzvp were employed. The first one is implemented in the *PRIRODA* program[S10] and two others in the *ORCA* program.[S11] Overall, the PBE/L1 method performed best matching experimental data (Table S7) with significantly lower computation times; calculation time for Hessian of **1** with PBE/L1+D3, r^{2}SCAN-3c,[S9] and PBE0-D3/def2-tzvp was 1, 12, and 60 min, respectively.

Table S7. Comparison of DFT-calculated ΔG with experimental ΔG_0 and $\Delta G^{\#}$, kJ mol^{-1}

Object	PBE/L1+D3	PBE/L1+D3[a]	r^{2}SCAN-3c	r^{2}SCAN-3c[b]	PBE0-D3/def2-tzvp	Exp.[c]
1-*tw*	0	–	–	–	0	0
1-*ch*	3.26				4.43	–0.13
1-TS	89.33				95.18	88.2
2-*tw*	0	0	0	0	0	0
2-*ch*	7.94	10.87	8.78	8.78	9.20	4.77
2-*ts*	61.45	79.84	64.37	56.4	68.55	69.47
2-TS	94.47	99.07	98.65	102.0	99.07	94.18
5-*tw*	0	–	–	–	0	0
5-*ch*	–5.64				4.18	–5.73
5-TS	87.57				94.26	90.46
RMS	3.68	7.48	4.56	9.07	4.43	–

[a] Minenkov's solvation model[S12] was used for the *PRIRODA* program.[S10] [b] CPCM solvation method implemented in the *ORCA* program.[S11] [c] In toluene solution.

3.2. Analysis of IRC trajectories

An IRC trajectory connects the TS with the corresponding minima, *i.e.*, reactant and product, on the potential energy surface. Analysis of the energy profile of the IRC trajectory allows for the discovery of additional special points, known as inflection points, referred to as hidden intermediates and hidden transition states. The identification of such points is in scope of interest because, when reaction conditions change, or when transitioning to related substrates, the hidden intermediate may become a true local minimum.[S13]

Distinct inflection points are observed on the IRC trajectory of the interconversion of *twist* conformers of compound **2**, corresponding to pronounced minima on the IRC gradient curve (Figure S8). These points correspond to the geometries *hi1a* and *hi1b* of the bent *twist* form. They are asymmetric, but if the non-planar state of the five-membered ring is not taken

into account, they have an effective C_2 rotation axis oriented vertically as shown in Figure 4. Geometries hi1a and *hi1b* represent hidden intermediates. Their characteristic *twistboat* conformations is the global minimum for 1,5-cyclooctadiene.[S14]

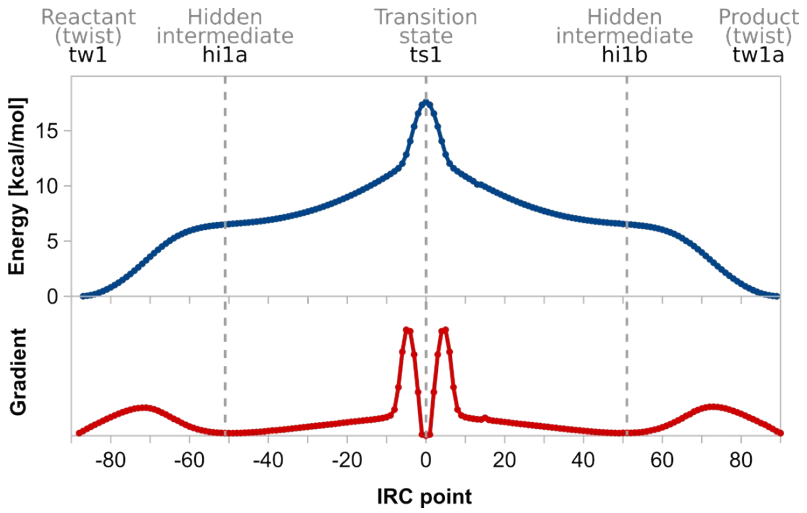

Figure S8 IRC trajectory of *twist-twist* interconversion of compound **2**; IRC step, 1.2 amu$^{1/2}$ Å.

Interestingly, the non-degenerate transformation *tw-ch* begins in the same path as the degenerate transformation *tw-tw* (Figures 4, S8). Both of these reactions pass through the same hidden intermediate *hi* with an effective C_2 symmetry. The system then enters a bifurcation point, and the reaction path splits into two valleys. One leads to the *ts1* with an increased symmetry to C_{2v}, whilst the other leads to the *TS2* with reduced symmetry to C_1.

The path of the non-degenerate transformation in the reverse direction, from *ch* to *TS2*, also passes through an inflection point, corresponding to a minimum on the IRC gradient plot (Figure S9). This C_s structure *HI* represents another hidden stationary point and is characterized as a *half-chair*.[S15] For the archetypal tetrathiocine **3** at the MP2/6-31G* [S15] and PBE/L1 levels of theory, a similar structure is a local minimum; whereas for compound **19** (for structure see Table S8), it represents the TS of the *chair* → *twist* process and vice versa (PBE/L1 and PBE0-D3/def2-tzvp). In cases where it is a hidden intermediate, the path from *hi* to TS branches into two symmetric valleys. Depending on which of the dihedral angles C–S–S–C in *hi* is distorted, a specific enantiomer's TS is obtained.

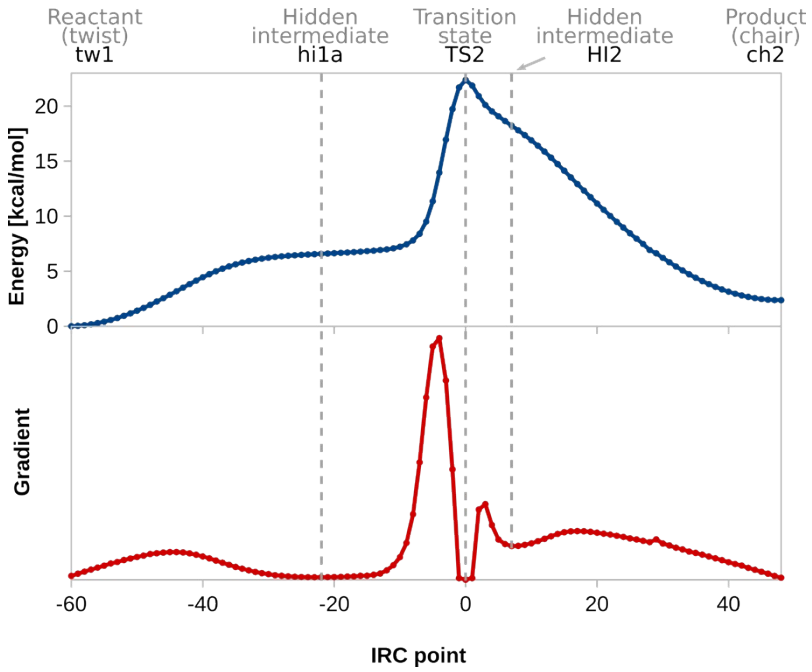

Figure S9 IRC trajectory of *twist-chair* transformation of compound **2**, IRC step 1.2 amu$^{1/2}$ Å.

3.3. Other calculations

Table S8. Calculated ΔG of the stationary points of compounds **1**, **4**, **5**, **18**-**20**, kcal mol^{-1} [a]

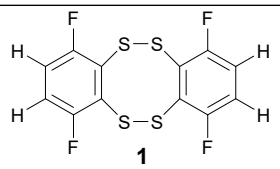

1

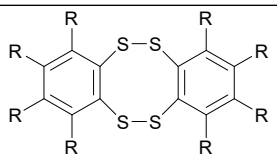

3 (R = F)
18 (R = Cl)
5 (R = H)

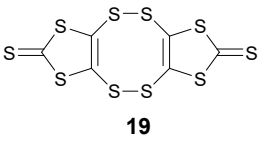

19

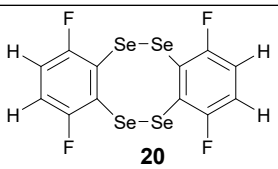

20

Stationary point	PBE/L1[b]	PBE0-D3/def2-tzvp
1-*tw*	0	0
1-*ch*	0.78	1.06
1-*ts*	13.74	15.61
1-TS	21.37	22.77
4-*tw*	0	0
4-*ch*	0.84	0.86
4-*ts*	14.32	15.55
4-TS	19.47	20.29
5-*tw*	0	0
5-*ch*	−1.35	−0.57
5-*ts*	11.52	13.75

5-TS	20.95	22.55
18-*tw*	0	0
18-*ch*	4.37	3.07
18-*ts*	15.45	15.63
18-TS	23.96	25.29
19-*tw*	0	0
19-*ch*	−2.56	−1.70
19-*ts*	6.91	10.02
19-TS	15.05	15.61
20-*tw*	0	0
20-*ch*	−2.59	−2.24
20-*ts*	8.89	9.22
20-TS	20.19	21.85

[a] Designations: *tw* – *twist* conformer, *ch* – *chair* conformer, *ts* – transition state of the racemization of *twist* conformer, TS – transition state of *twist* → *chair* transformation [b] With Grimme's D3 dispersion correction to optimized geometry.

4. Kinetics evaluation

4.1. Equilibrium *chair* ↔ *twist*

Equation $\Delta G = -RTlnK$ in the form y = x*ΔH + ΔS; K = twist/chair, x = −1000/T; y = R*ln(K), ΔG = y/x (Tables S9-S13; calorie is used as energy unit).

Table S9. Compound **1** in toluene solution

T	K	x	y	ΔG_0
302.2	0.952	−3.309	−0.098	0.0295
301.5	0.949	−3.317	−0.105	0.0316
301.0	0.947	−3.322	−0.109	0.0328
295.1	0.936	−3.389	−0.131	0.0385
295.0	0.935	−3.390	−0.133	0.0393
313.4	0.974	−3.191	−0.053	0.0167
313.3	0.979	−3.192	−0.042	0.0133
323.0	0.982	−3.096	−0.036	0.0116
322.9	0.981	−3.097	−0.039	0.0126
332.6	0.991	−3.007	−0.019	0.0063

332.6	0.978	−3.007	−0.045	0.0148
342.2	0.981	−2.922	−0.038	0.0131
342.3	0.963	−2.921	−0.076	0.0260
351.9	0.969	−2.842	−0.064	0.0224
351.9	0.956	−2.842	−0.089	0.0314
361.5	0.968	−2.766	−0.065	0.0236
361.5	0.947	−2.766	−0.108	0.0389
371.2	0.95	−2.694	−0.103	0.0381
376.0	0.95	−2.660	−0.102	0.0384
310.2	0.966	−3.224	−0.069	0.0215

Table S10. Compound **1** in chloroform solution

T	K	x	y	ΔG_0
332.7	1.15	−3.006	0.284	−0.0946
322.9	1.20	−3.097	0.361	−0.1165
313.3	1.22	−3.192	0.401	−0.1257
300.9	1.26	−3.323	0.452	−0.1360
295.3	1.28	−3.386	0.487	−0.1438

Table S11. Compound **2**

T	K	x	y	ΔG_0
296.9	6.88	−3.368	3.833	−1.1379
304.8	6.82	−3.281	3.815	−1.1629
313.5	6.64	−3.190	3.762	−1.1794
323.0	6.34	−3.096	3.670	−1.1855
332.7	6.20	−3.006	3.626	−1.2063
342.3	5.94	−2.921	3.541	−1.2120
351.9	5.74	−2.842	3.473	−1.2220
361.6	5.48	−2.765	3.380	−1.2224
371.3	5.24	−2.693	3.291	−1.2221
376.0	5.13	−2.660	3.249	−1.2217
380.8	5.06	−2.626	3.222	−1.2269
295.6	6.88	-3.383	3.834	−1.1333
332.6	6.19	−3.007	3.623	−1.2050
342.2	5.99	−2.922	3.558	−1.2176
351.9	5.76	−2.842	3.480	−1.2245
361.5	5.52	−2.766	3.393	−1.2267
371.2	5.26	−2.694	3.301	−1.2252
376.0	5.17	−2.660	3.264	−1.2274

322.7	6.60	−3.099	3.750	−1.2102
304.2	6.78	−3.287	3.803	−1.1569

Table S12. Compound **5**[S2]

T	K	x	y	ΔG_0
300.0	0.100	−3.333	−4.58	1.373
310.0	0.117	−3.226	−4.26	1.322
320.0	0.123	−3.125	−4.16	1.333
330.0	0.153	−3.030	−3.73	1.231
340.0	0.157	−2.941	−3.68	1.251
350.0	0.181	−2.857	−3.40	1.189
360.0	0.201	−2.778	−3.19	1.148
370.0	0.215	−2.703	−3.05	1.130
380.0	0.226	−2.632	−2.96	1.123

Table S13. Compound **5**, this work

T	K	x	y	ΔG_0
296.3	0.107	−3.375	−4.45	1.3174
313.4	0.123	−3.191	−4.16	1.3043
323.0	0.14	−3.096	−3.91	1.2635
332.6	0.148	−3.007	−3.79	1.2615
342.3	0.16	−2.921	−3.65	1.2486
351.9	0.173	−2.842	−3.49	1.2286
361.6	0.179	−2.765	−3.41	1.2346
371.2	0.184	−2.694	−3.36	1.2469
376.0	0.188	−2.660	−3.32	1.2486
307.2	0.125	−3.255	−4.13	1.2697

Compound **1** in toluene: ΔH_0 = 0.1 ± 0.14 kJ mol^{-1}, ΔS_0 = 0.04 ± 0.4 J K^{-1} mol^{-1}, r = 0.200.

Compound **1** in chloroform: ΔH_0 = −2.1 ± 0.2 kJ mol^{-1}, ΔS_0 = −5.0 ± 0.6 J K^{-1} mol^{-1}, r = -0.988.

Compound **2**: ΔH_0 = −3.53 ± 0.15 kJ mol^{-1}, 4.4 ± 0.5 J K^{-1} mol^{-1}, r = 0.983.

Compound **5**[S2]: ΔH_0 = 9.9 ± 0.4 kJ mol^{-1}, ΔS_0 = 14 ± 1 J K^{-1} mol^{-1}, r = 0.994.

Compound **5**, this work: ΔH_0 = 6.5 ± 0.3 kJ mol^{-1}, ΔS_0 = 3.8 ± 0.9 J K^{-1} mol^{-1}, r = 0.9915.

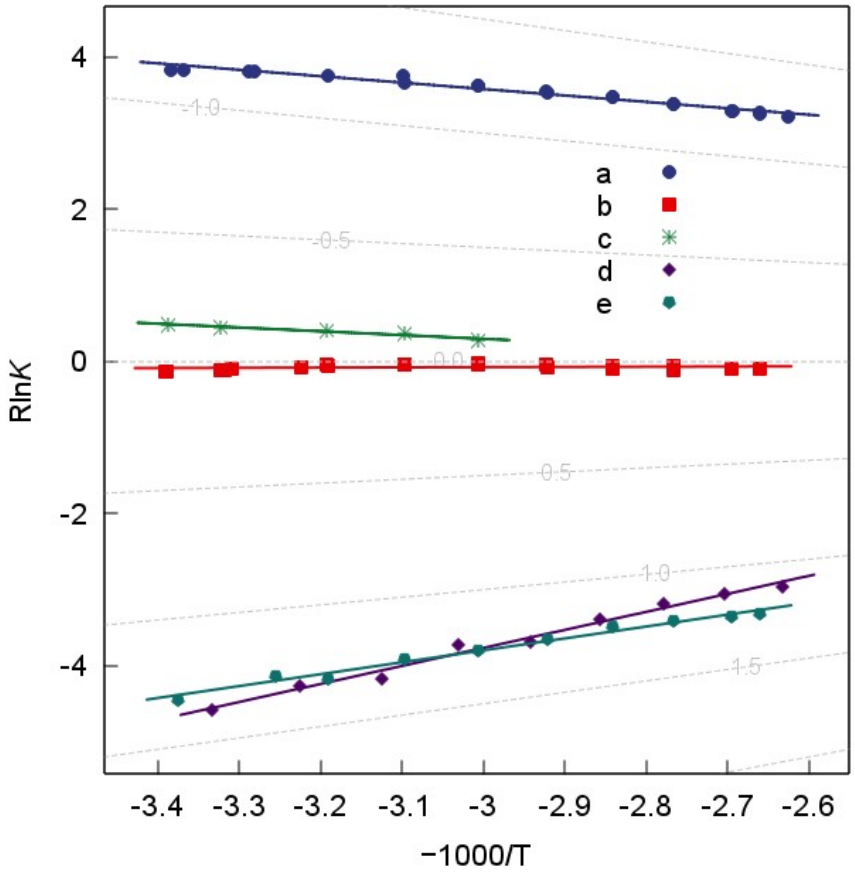

Figure S10 Temperature dependence of the conformational equilibrium constants for **1** (*b*: in toluene, red squares; *c*: in chloroform solution, green stars), **2** (*a*: blue circles), and **5** (*d*: purple diamonds;[S2] *e*: blue-green pentagons, this work); dashed lines are *ΔG* isolines.

4.2 *Twist* → *twist* and *chair* → *twist* kinetics

Eyring equation in the form y = x**ΔH* + *ΔS*; x = −1000/T, y = R*(ln(k/T) − 23.76), *ΔG* = y/x (Tables S14-S18; calorie is used as energy unit).

Table S14. Compound **1** in toluene, *chair* → *twist*

T	k	x	y	$\Delta G^{\#}$
313.3	0.015	−3.192	−67.0	20.986
322.9	0.054	−3.097	−64.5	20.826
332.6	0.175	−3.007	−62.2	20.694

342.2	0.529	−2.922	−60.1	20.559
351.9	1.45	−2.842	−58.1	20.456
361.5	3.72	−2.766	−56.3	20.356
371.2	8.93	−2.694	−54.6	20.276
376.0	12.4	−2.660	−54.0	20.305
376.0	15.3	−2.660	−53.6	20.146
371.2	10.5	−2.694	−54.3	20.157
361.5	3.53	−2.766	−56.4	20.394

Table S15. Compound **1** in $CDCl_3$, *chair* → *twist*

T	k	x	y	$\Delta G^{\#}$
332.7	0.18	−3.006	−62.16	20.682
322.9	0.04	−3.097	−65.09	21.019
313.2	0.008	−3.193	−68.23	21.370

Table S16. Compound **2**, *twist* → *twist*

T	k	x	y	$\Delta G^{\#}$
304.8	8.6	−3.281	−54.3	16.55
323.0	79	−3.096	−50.0	16.15
332.7	178	−3.006	−48.5	16.12
342.3	418	−2.921	−46.8	16.03
351.9	961	−2.842	−45.2	15.91
361.6	2280	−2.765	−43.6	15.75
371.3	4810	−2.693	−42.1	15.64
376.0	6550	−2.660	−41.5	15.62
380.8	8920	−2.626	−40.9	15.59
304.8	6.9	−3.281	−54.7	16.69
313.5	22	−3.190	−52.5	16.46
323.0	78.5	−3.096	−50.0	16.16
332.7	194	−3.006	−48.3	16.07

Table S17. Compound **2**, *chair* → *twist*

T	k	x	y	$\Delta G^{\#}$
371.3	5.1	−2.693	−55.74	20.695
376.0	8.85	−2.660	−54.67	20.555
376.0	9.14	−2.660	−54.60	20.530
376.0	8.08	−2.660	−54.85	20.623
376.0	7.1	−2.660	−55.10	20.719
380.8	10.1	−2.626	−54.43	20.727
332.5	0.096	−3.008	−63.41	21.084
342.3	0.3	−2.921	−61.21	20.951
351.9	0.84	−2.842	−59.21	20.837
361.5	2.25	−2.766	−57.31	20.717
371.2	5.84	−2.694	−55.47	20.589
376.0	8.24	−2.660	−54.81	20.608

Table S18. Compound **5**, *chair* → *twist*

T	k	x	y	$\Delta G^{\#}$
332.7	0.0072	−3.006	−68.56	22.810
342.2	0.0196	−2.922	−66.63	22.799
351.9	0.0584	−2.842	−64.51	22.702
361.6	0.147	−2.765	−62.73	22.682
371.2	0.352	−2.694	−61.05	22.661
376.0	0.531	−2.660	−60.26	22.656

Compound **1** in toluene, *chair* → *twist*: $\Delta H^{\#}$ = 103.5 ± 1.1 kJ mol^{-1}, $\Delta S^{\#}$ = 51 ± 3 J K^{-1} mol^{-1}, r = 0.999.

Compound **1** in $CDCl_3$, *chair* → *twist*: $\Delta H^{\#}$ = 135.6±0.7 kJ mol^{-1}, $\Delta S^{\#}$ = 148 ± 2 J K^{-1} mol^{-1}, r = 0.999986.

Compound **2**, *twist* → *twist*: $\Delta H^{\#}$ = 86.2 ± 1.4 kJ mol^{-1}, $\Delta S^{\#}$ = 56 ± 4 J K^{-1} mol^{-1}, r = 0.999.

Compound **2**, *chair* → *twist*: $\Delta H^{\#}$ = 101.6 ± 2.1 kJ mol^{-1}, $\Delta S^{\#}$ = 41 ± 6 J K^{-1} mol^{-1}, r = 0.998.

Compound **5**, *chair* → *twist*: $\Delta H^{\#}$ = 101 ± 1 kJ mol^{-1}, $\Delta S^{\#}$ = 17 ± 3 J K^{-1} mol^{-1}, r = 0.99983.

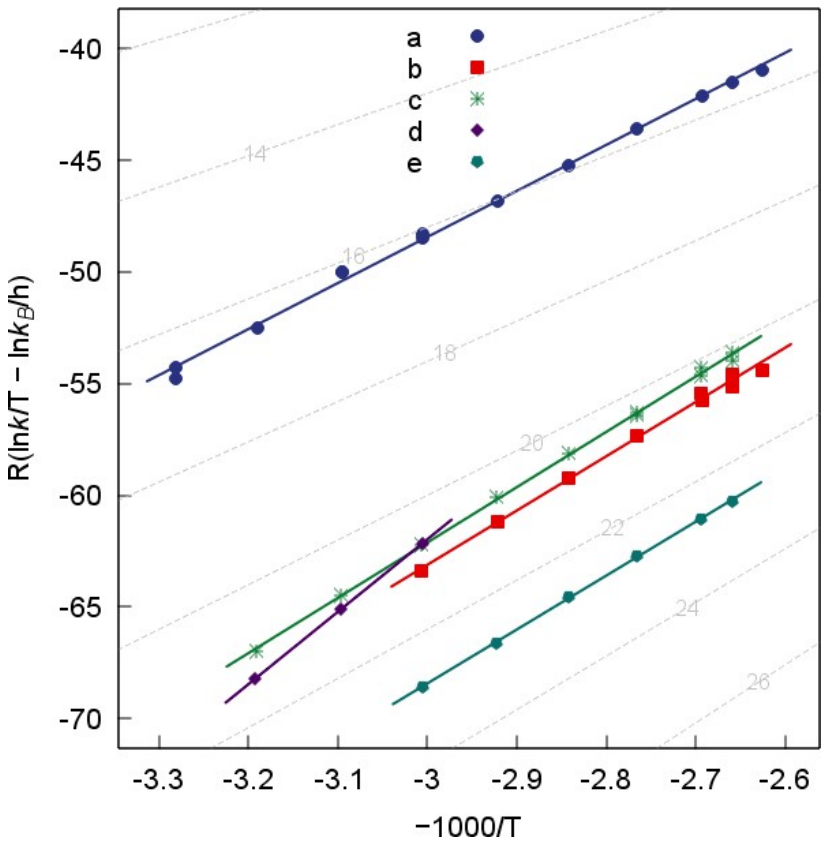

Figure S11 Temperature dependence of the rates of transitions *chair* → *twist* for **1** (*c*: green stars; *d*: in chloroform solution, purple diamonds), **2** (*b*: red squares), and **5** (*e*: blue-green pentagons), and *twist* → *twist* for **2** (*a*: blue circles); dashed lines are $\Delta G^{\#}$ isolines.

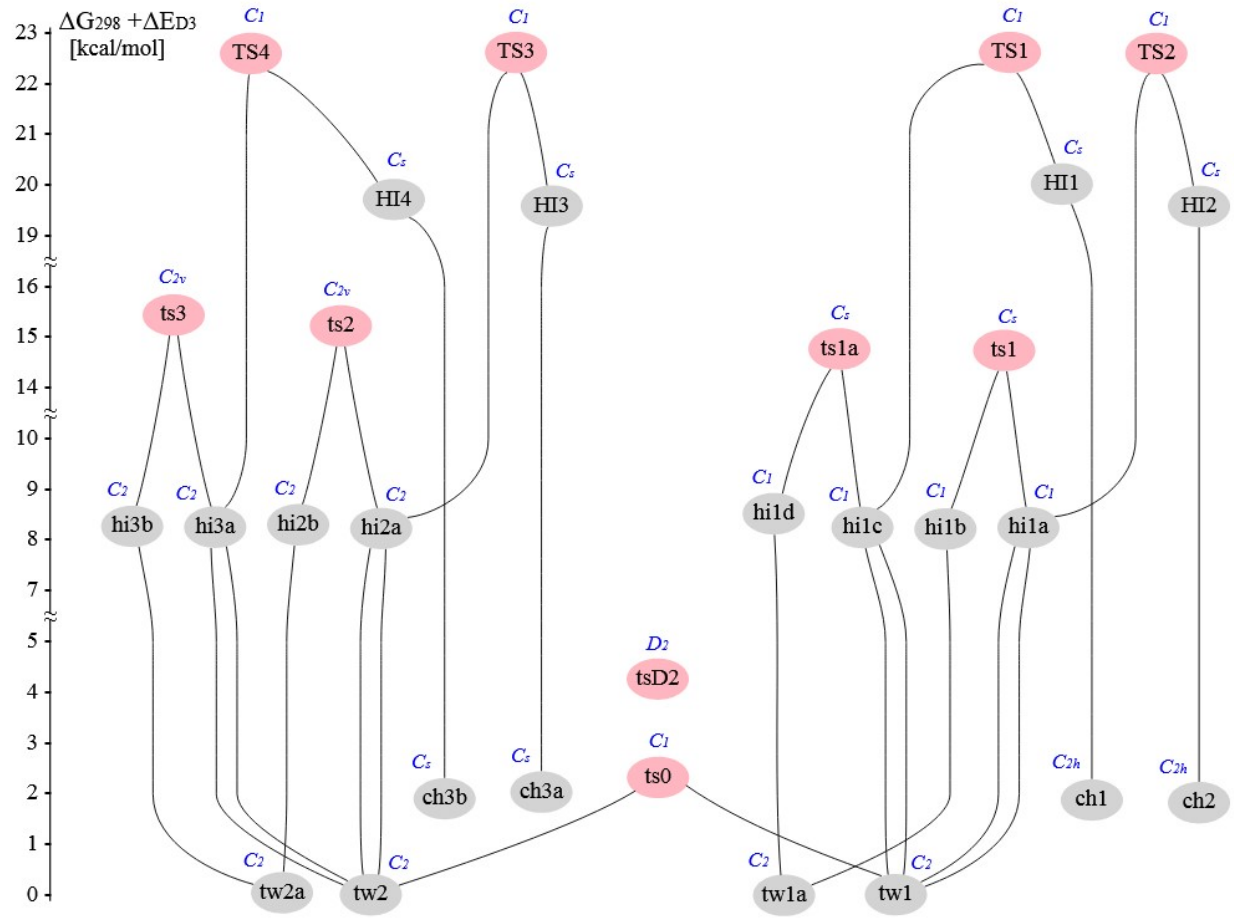

Figure S12 Energy diagram for stable conformations, transition states and intermediates for **2**. 3D visualization and xyz-coordinates of all structures are available at the website http://limor1.nioch.nsc.ru/quant/Makarov/tetrathiocin/

5. References

S1 E. J. Yearley, E. L. Lippert, D. J. Mitchell and A. A. Pinkerton, *Acta Crystallogr. C*, 2007, **63**, o576–o577

S2 T. Chivers, M. Parvez, I. Vargas-Baca and G. Schatte, *Can. J. Chem.*, 1998, **76**, 1093–1101.

S3 W. R. Dolbier, in: *Guide to Fluorine NMR for Organic Chemists*, Wiley, 2009.

S4 S. A. Ukhanev, S. V. Fedorov, Yu. Yu. Rusakov, I. L. Rusakova and L. B. Krivdin, *J. Fluor. Chem*., 2023, **266**, 110093.

S5 J. W. Emsley, J. Feeney and L. H. Sutcliffe, *High Resolution Nuclear Magnetic Resonance Spectroscopy*, Vol. 1, Pergamon Press, 1965.

S6 D. A. Cheshkov, K. F. Sheberstov, D. O. Sinitsyn and V. A. Chertkov, *Magn. Reson. Chem.*, 2018, **56**, 449–457.

S7 W. D. Arnold, J. Mao, H. Sun and E. Oldfield, *J. Am. Chem. Soc.*, 2000, **122**, 12164–12168.

S8 J.-C. Hierso, *Chem. Rev.*, 2014, **114**, 4838–4867.

S9 J. W. Furness, A. D. Kaplan, J. Ning, J. P. Perdew and J. Sun, *J. Phys. Chem. Lett.*, 2020, **110**, 8208–8215.

S10 D. N. Laikov and Yu. A. Ustynyuk, *Russ. Chem. Bull.*, 2005, **54**, 820–826.

S11 F. Neese, *WIREs Comput. Mol. Sci.*, 2022, **120**, e1606.

S12 Y. Minenkov, J. *Chem. Theory Comput.*, 2023, **19**, 5221–5230.

S13 E. Kraka and D. Cremer, *Acc. Chem. Res.*, 2010, **43**, 591–601.

S14 W. R. Rocha and W. B. De Almeida, *J. Comput. Chem.*, 1997, **18**, 254–259.

S15 T. Shimizu, K. Iwata, N. Kamigata and S. Ikuta, *J. Chem. Res.*, 1997, 38–39.